# Power Losses and Thermal Modeling of a 4H-SiC VJFET Inverter

Hui Zhang[1], Leon M. Tolbert[1,2], Burak Ozpineci[2], Madhu S. Chinthavali[2]
hzhang18@utk.edu, tolbert@utk.edu, ozpinecib@ornl.gov, chinthavalim@ornl.gov

[1]Electrical and Computer Engineering
The University of Tennessee
Knoxville, TN 37996-2100

[2] Power Electronics & Electric Machinery Research Center
Oak Ridge National Laboratory
Knoxville, TN 37932

***Abstract*—This paper presents a set of models for a SiC VJFET inverter from device level to system level. The simulations for SiC and Si inverters indicated that the SiC inverter has a much lower junction temperature, much less power loss, significantly enhanced energy efficiency, and a dramatic reduction in heatsink size as compared with the Si inverter. This demonstrated the technical feasibility and benefits of the all-SiC inverter. In addition to the simulations, experimental tests have also been conducted on SiC VJFETs and Schottky diodes for parameter extraction.**

***Keywords* — Silicon Carbide (SiC), VJFET, Schottky diode, inverter, power loss modeling, thermal modeling.**

## I. Introduction

Silicon carbide (SiC) is a wide bandgap semiconductor. It has many good properties such as large bandgap, large breakdown electric field, high electron saturated velocity, and high thermal conductivity. These merits can result in good performances of semiconductor devices under high-power, high-frequency, and high-temperature conditions. Thus, SiC has been envisioned as the material of choice for the next-generation power devices.

SiC exists as several polytypes that have different stacking sequence of double layers of silicon and carbon atoms and resultant different properties. Table I shows the electrical and material properties of three polytypes, namely 4H-SiC, 6H-SiC, and 3C-SiC. Among these three polytypes, 4H-SiC is particularly suited for vertical power devices because of its higher vertical (*c*-axis) mobility. Furthermore, its large bandgap energy is also expected to result in a higher operating temperature and higher radiation hardness than the others.

At present, most commercially available SiC devices are Schottky diodes. The main manufacturers are CREE, SemiSouth Laboratories, Advanced Power Technology, Infineon, SiCED, and Rockwell Scientific. They can provide SiC Schottky diodes at 600V or 1200V rating, up to a current rating of 20 A. (Research prototypes have been demonstrated at currents of up to 100 A.) Besides SiC Schottky diodes, SemiSouth Laboratories has begun to provide SiC VJFETs (HEL2FET™, 600V/2A). SiCED also demonstrated their cascode prototype of SiC VJFET (1500V/3A, 1300V/2A). All of the other SiC devices, like SiC MOSFETs, are still in the realm of research prototypes.

In this paper, a three-phase full-bridge inverter as shown in Fig. 1 is studied. It is composed of six 4H-SiC VJFETs, each of which has an anti-parallel Schottky diode. These VJFETs are driven by a three-phase PWM signal. Device on-state resistance models and system power loss models are developed, and applied into the simulation study of this inverter under a specific servo drive condition. These models can reflect the change of system performance with temperature, and also the heatsink size can be estimated. The simulation results demonstrated dramatic improvement of a SiC inverter compared to its Si counterpart.

TABLE I. Si/SiC ELECTRICAL AND MATERIAL PROPERTIES

| **Property** | ***Si*** | ***4H-SiC*** | ***6H-SiC*** | ***3C-SiC*** |
|---|---|---|---|---|
| Bandgap, $E_g$ (eV) | 1.11 | 3.26 | 2.86 | 2.2 |
| Breakdown electric field, $E_c$ (kV/cm) | 300 | 2200 | 2500 | 1200 |
| Relative dielectric constant, $\varepsilon_r$ | 11.8 | 10.1 | 9.7 | 9.66 |
| Electron mobility, $\mu_n$ (cm$^2$/V·s) | 1350 | 950<br>800 | 500<br>80 | 900 |
| Saturated Electron Drift Velocity, $v_{sat}$ (cm/s) | $1\times10^7$ | $2\times10^7$ | $2\times10^7$ | $2.5\times10^7$ |
| Thermal conductivity, $R_{th}$ (W/cm·K) | 1.5 | 4.9 | 4.9 | 4.9 |

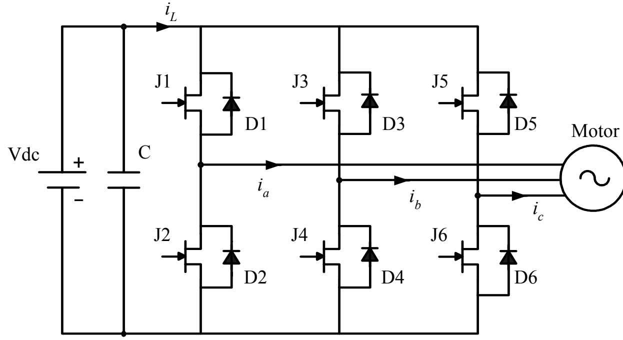

Fig. 1. Standard 3-phase inverter.

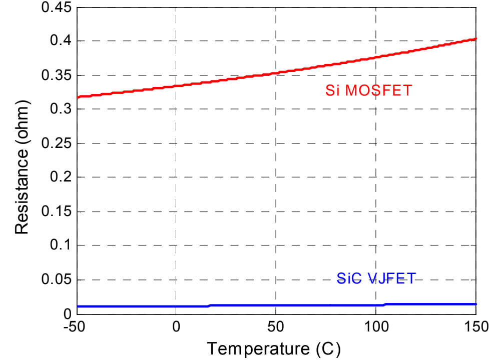

Fig. 2. Drift resistances of SiC VJFET and Si MOSFET.

## II. Modeling of the On-State Resistance

VJFETs and Schottky diodes are both majority carrier devices. Their on-state specific resistances can be represented as

$$R_{on,sp} = \frac{4V_B^2}{\varepsilon E_c^3 \mu_n}, \tag{1}$$

where $V_B$ is the breakdown voltage which is determined by the application requirements. $\varepsilon$, $E_c$, and $\mu_n$ are dependent on material. $\mu_n$ is also influenced by several other factors.

By Caughey and Thomas' model [1, 2], $\mu_n$ is dependent on doping density as shown in (2). This model counts the combined lattice and ionized impurity mobility. Another model reported by Sabnis and Clemens [2] considers the mobility due to carrier heating and is shown in (3). It reflects the effects of applied electrical field and saturation velocity. Please refer to the Appendix at the end of this paper for symbol definitions.

$$\mu_0 = \mu_{\min} + \frac{\mu_{\max} - \mu_{\min}}{1 + \left(N_{tot}/N_{ref}\right)^{\alpha}} \tag{2}$$

$$\mu_n(E) = \frac{\mu_0}{\left\{1 + \left|\frac{\mu_0 E}{v_s}\right|^{\beta}\right\}^{1/\beta}} \tag{3}$$

where $\alpha$ and $\beta$ are empirical coefficients (refer to Table II).

In (2) and (3), $\mu_{max}$, $\mu_{min}$, $N_{ref}$, and $v_s$ are temperature-dependent. They can be approximated using simple power expressions of temperature, as shown in (4) – (6). $A_{\mu_{\max}}$, $A_{\mu_{\min}}$, $A_{N_{ref}}$, $B_{\mu_{\max}}$, and $B_{\mu_{\min}}$ are the parameters that can be obtained by fitting experimental data. Thus, the electron mobility is a function of temperature, and so is the on-state resistance.

$$\mu_{\max} = A_{\mu_{\max}} \times \left(\frac{T}{300}\right)^{-B_{\mu_{\max}}} \tag{4}$$

$$\mu_{\min} = A_{\mu_{\min}} \times \left(\frac{T}{300}\right)^{-B_{\mu_{\min}}} \tag{5}$$

$$N_{ref} = A_{N_{ref}} \times \left(\frac{T}{300}\right) \tag{6}$$

Combining Caughey and Thomas' model with Sabnis and Clemens' model, the resistances can be estimated more exactly. Fig. 2 shows the resistances of similar rating SiC VJFET and Si MOSFET computed in this way using the values in Table II. The SiC VJFET shows more than 100 times advantage in drift resistance compared to that of a Si MOSFET. This is attributed to its higher doping density and thinner blocking layer thickness.

## III. System Power Loss Model

Based on the resistance model, an averaging technique was employed to set up a system power loss model. This technique averages all variables in a switching cycle and uses these average values as a sampling point for a new model. It has been proven to work well in the estimation of the behavior of an inverter previously [3].

The total power loss of this system is equal to the sum of the power losses of each VJFET and Schottky diode. Both the power losses of the VJFET and diode are composed of conduction loss ($P_{cond,J}$, $P_{cond,D}$) and switching loss ($P_{sw,J}$, $P_{sw,D}$). The only difference is that the conduction loss of the VJFET has an additional part ($P_{cond,D\to J}$) that is due to diode's reverse recovery current. Applying the averaging technique, it is easy to obtain the expressions of conduction losses as follows:

$$P_{cond,J} = I^2 \cdot R_{DS,on}\left(\frac{1}{8} + \frac{1}{3\pi} M \cos\phi\right), \tag{7}$$

$$P_{cond,D\to J}=\left(\frac{dI_R}{dt}\right)^2\cdot\frac{f_c t_{rr}^{\ 3}}{3(S+1)^2}\cdot R_{DS,on}\ ,\qquad (8)$$

$$P_{cond,D}=I^2\cdot R_D\left(\frac{1}{8}-\frac{1}{3\pi}M\cos\phi\right)+I\cdot V_D\cdot\left(\frac{1}{2\pi}-\frac{M\cos\phi}{8}\right)\ ,\qquad (9)$$

where $S$ is snappiness factor and is defined in [3] .

A normally-on VJFET is somewhat similar to a MOSFET as far as its switching characteristics are concerned. It is reasonable to use the model in [4] to estimate the VJFET's switching performance. Combined with the averaging technique, its switching loss can be computed by

$$P_{sw,J}=\frac{Hf_c}{2\pi}\left\{\begin{aligned}&\frac{G_1}{\sqrt{G_1^{\ 2}-J'^2}}\left[\pi+2\tan^{-1}\left(\frac{J'}{\sqrt{G_1^{\ 2}-J'^2}}\right)\right]\\&+\frac{G_2}{\sqrt{G_2^{\ 2}-J'^2}}\left[-\pi+2\tan^{-1}\left(\frac{J'}{\sqrt{G_2^{\ 2}-J'^2}}\right)\right]\end{aligned}\right\},\qquad (10)$$

where $J'=\dfrac{I}{A}$, $H=\dfrac{1}{3}\varepsilon E_c VA\left(\dfrac{V}{V_B}\right)^{1/2}$, $G_1=g_m(V_{GH}-V_{th})$, and $G_2=g_m(V_{th}-V_{GL})$.

For a Schottky diode, the reverse recovery loss dominates its switching losses. So in this model, the other switching losses are neglected and only reverse recovery loss is considered for the switching loss:

$$P_{sw,D}=f_c\cdot\frac{V_R}{2S}\left(\frac{dI_R}{dt}\right)\left(\frac{St_{rr}}{S+1}\right)^2.\qquad (11)$$

## IV. Thermal Modeling

Thermal modeling is used to estimate the device performance under different temperatures. Using the equivalent circuit is an effective way. Fig. 3 shows a single device thermal equivalent circuit from junction to case originated from a finite difference discretization of the heat equation, where $T_j(t)$, $T_c(t)$, and $P(t)$ are junction temperature, case temperature, and power dissipation at time $t$, respectively. The basic mathematical expression of this circuit can be represented as

$$Z_{jc}(s)=\frac{R_1}{1+s\tau_1}+\frac{R_2}{1+s\tau_2}+\cdots+\frac{R_n}{1+s\tau_n}\ ,\qquad (12)$$

where $\tau_i = R_iC_i$ ($i$ = 1, 2, …, $n$) and the sum of $R_i$ is equal to the junction-case thermal resistance, $R_{jc}$. Usually, $n$ = 2 sufficiently approximates experimental results [5].

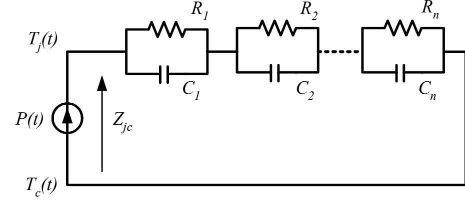


Fig. 3. Junction-case thermal equivalent circuit.

Applying this method into the analysis of the inverter system, the system thermal model is obtained, which is shown as Fig. 4. $P_j(t)$ and $P_d(t)$ are the total power losses generated by a VJFET and a Schottky diode, respectively. Assume the VJFET and the Schottky diode are mounted on the same heatsink. Then the power losses $P_j(t)$ and $P_d(t)$ flow through separate paths from their own junction to case, where the temperatures are equal for contacting to the same heatsink. Afterwards, they merge with each other ($P_j(t)$+$P_d(t)$) and flow together through the heatsink to atmosphere. This forms two separate thermal loops, as shown as Fig. 4.

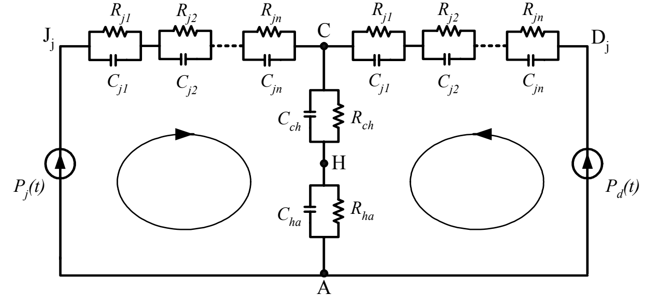


Fig. 4. Thermal equivalent circuit of inverter module.

## V. Simulation and Analysis

Using the above models, an inverter used in a servo drive system (shown in Fig. 1) is simulated. For the purpose of comparison between SiC and Si inverters, the same simulation was also done for a comparable Si inverter. The key parameters used here are listed in Table II.

TABLE II. SIMULATION PARAMETERS

| Property | *4H-SiC* | *Si* |
|---|---|---|
| Breakdown electric field, $E_c$ (kV/cm) | 2200 | 300 |
| Relative dielectric constant, $\varepsilon$ | 10.1 | 11.9 |
| Doping coefficient of $\mu$, $\alpha$ | 0.76 | 0.91 |
| Electric field coefficient of $\mu$, $\beta$ | 1 | 2 |
| Coefficient of $\mu_{\max}$, $A_{\mu_{\max}}$ | 950 | 1350 |
| Coefficient of $\mu_{\max}$, $B_{\mu_{\max}}$ | 2.4 | 2.5 |
| Coefficient of $\mu_{\min}$, $A_{\mu_{\min}}$ | 40 | 92 |
| Coefficient of $\mu_{\min}$, $B_{\mu_{\min}}$ | 0.5 | 0.91 |
| Coefficient of $N_{ref}$, $A_{N_{ref}}$ | $2\times10^{17}$ | $1.3\times10^{17}$ |
| Maximum saturated velocity, $v_{s\max}$ (cm/s) | $4.77\times10^{7}$ | $2.4\times10^{7}$ |

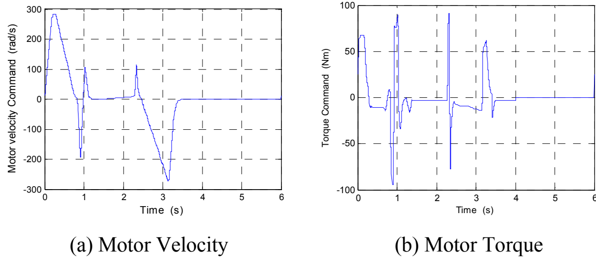


(a) Motor Velocity (b) Motor Torque

Fig. 5. Servo drive system command.

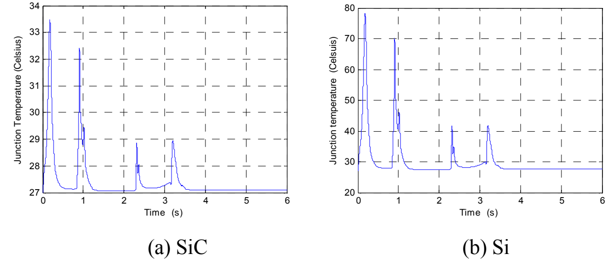


(a) SiC (b) Si

Fig. 6. Junction temperature of VJFETs.

This drive system is required to perform the function shown in Fig. 5. The switching frequency is 20 kHz. Assume the ambient temperature is 27°C and the thermal considerations are $R_{ch}$ = 0.0026 K/W, $\tau_{ch}$ = 0.01 s (for grease) and $R_{ha}$ = 1 K/W, $\tau_{ch}$ = 900 s (for heatsink). Then, the junction temperatures of the SiC and Si devices are as shown in Fig. 6 and Fig. 7. The junction temperatures of the SiC devices are significantly less than those of the Si devices.

Table III lists some detailed information under two different cooling conditions. Heatsink 1 is the best available aluminum heatsink without a fan, while Heatsink 2 is the best available aluminum heatsink with a fan. Except for the obvious smaller peak temperature of the SiC device, the temperature rise per cycle is also dramatically smaller than that of the Si device. This means that SiC devices can operate safely for much longer continuous time under the same temperature limit. The table also demonstrates that the better thermal management makes a significant contribution to the reduction of an average junction temperature rise, particularly for the SiC devices.

Changing from Heatsink 1 to Heatsink 2, the average junction temperature rise is reduced by a factor of 6.4 for SiC VJFETs and 3.1 for SiC diodes. This is mainly due to the relatively high thermal conductance of the SiC material. However, cooling conditions cannot change the peak junction temperatures much because the peak values are mainly determined by device packaging and material. These facts lead to the conclusion that the SiC inverter has better tolerance to high temperature and is possible to work well in a longer term with a good cooling condition than the Si inverter.

The SiC inverter is more efficient than the Si inverter. On one hand, it has lower power loss, which is about 1/7th of that of the Si inverter, and in turn has an 8 % points advantage in efficiency – 98.74 % compared to 90.79 % (refer to Table IV).

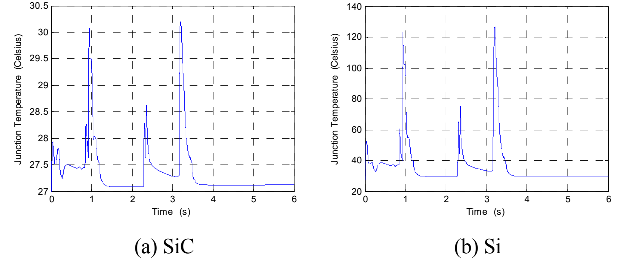


(a) SiC (b) Si

Fig. 7. Junction temperature of Schottky diodes.

In addition, the size of the heatsink of the SiC inverter is significantly reduced under the same temperature limit, which is the result of lower power dissipation and good thermal characteristics. For example, if the SiC inverter operates with Heatsink 1, by Table III its temperature rise per cycle should be 0.096 °C, and that of the Si inverter with the same heatsink should be 0.727 °C. Now, reducing this to 0.096 °C, the size of the heatsink for Si must be increased to 8 times of the original one. See Table V.

TABLE IV. AVERAGE POWER LOSS AND EFFICIENCY OF SIC/SI INVERTER

| Material | *Average power input (W)* | *Average power loss (W)* | *Inverter efficiency (%)* |
|---|---|---|---|
| SiC | 1131.21 | 14.21 | 98.74 |
| Si | 1131.21 | 104.13 | 90.79 |

TABLE V. SIZES OF HEATSINKS FOR SIC AND SI DEVICES

| Device | *Volume ($cm^3$)* | *Mass (g)* |
|---|---|---|
| SiC inverter | 337 | 935 |
| Si inverter | 2624 | 7269 |

*Aluminum 2024-T3: heat capacity 963 J/kg·K, density 2770kg/cm3

TABLE III. JUNCTION TEMPERATURE AND POWER LOSS

| **Material** <br> ***R* (K/W), $\tau$ (s)** | | **Maximum temperature for 1st cycle (°C)** | | **Avg. temperature rise per cycle (°C)** | | **Maximum power loss (W)** |
|---|---|---|---|---|---|---|
| | | ***VJFETs*** | ***Diodes*** | ***VJFETs*** | ***Diodes*** | |
| Heatsink 1, $R_{ch}$= 0.0026, $\tau_{ch}$ =0.01, $R_{ha}$= 1, $\tau_{ha}$ = 900 | SiC | 33.473 | 30.201 | 0.096 | 0.121 | 224.41 |
| | Si | 78.171 | 126.479 | 0.727 | 2.836 | 1913.8 |
| Heatsink 2, $R_{ch}$= 0.0026, $\tau_{ch}$ =0.01, $R_{ha}$= 0.01, $\tau_{ha}$ = 60 | SiC | 33.456 | 30.130 | 0.015 | 0.039 | 224.41 |
| | Si | 78.032 | 125.926 | 0.133 | 2.241 | 1913.8 |

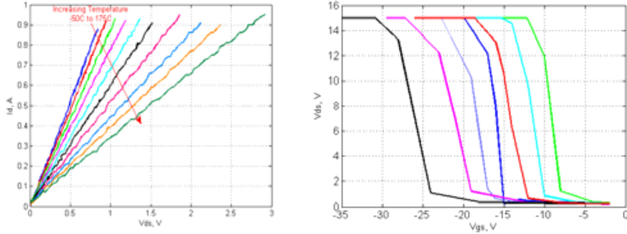

(a) I-V curve at different temperatures (b) Transfer characteristics

Fig. 8. Test characteristics of SiC VJFET (1200V/2A).

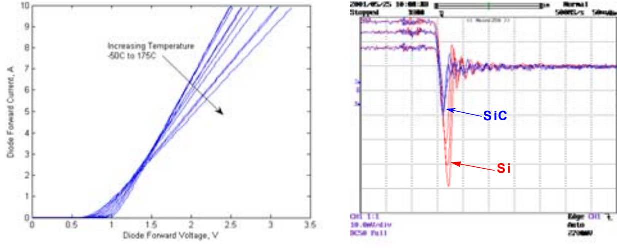


(a) I-V curve at different temperatures (b) Turn off waveforms (2A/div)

Fig. 9. Test characteristics of SiC Schottky diode.

## VI. Device Tests

In addition to the simulations, some tests have been conducted on SiC VJFETs and Schottky diodes for parameter extraction that was used in the simulations. A normally-on SiC VJFET rated at 1200 V and 2 A was tested to study the high temperature behavior of the device [7]. The forward characteristics of this device at different temperatures are shown in Fig. 8(a). The reciprocals of the slopes are the on-resistance of the VJFET, which increases from 0.36 Ω at -50°C to 1.4 Ω at 175°C. It indicates that SiC VJFETs have positive temperature coefficient. This is a desirable property for paralleling of devices in high current applications. For the servo drive system presented in this paper, about 10 SiC VJFETs were paralleled to meet the system requirements.

Fig. 8(b) shows the transfer characteristics of different VJFET samples. The pinch-off voltage of each sample can be read from the figure. It is an important parameter which determines the design of the gate drive circuit, such as the levels of gate voltages. Also, these values have significant influence on the switching loss of the VJFET. The relationship is reflected in the model by (10).

Characteristics of SiC Schottky diodes are shown in Fig. 9. Fig. 9(a) shows the I-V characteristics of SiC Schottky diodes. As shown in the figure, the forward voltage drop has two components, one is a constant part (for certain temperature) at low current levels that is defined as $V_D$ in the models, and the other is linear current-dependent part above $V_D$. $V_D$ decreases as temperature increases and affects conduction loss of the SiC Schottky diodes, referring to (9). Fig. 9(b) is the turn off waveforms of SiC and Si Schottky diodes for different forward current values [7]. The reverse recovery currents of the Si Schottky diode are dramatically larger than that of the SiC Schottky diode. This is a main contribution to the large switching loss of a Si Schottky diode. The reverse recovery current of a Si Schottky diode is also affected by its forward current. It increases as forward current increases, while for SiC Schottky diodes, the reverse recovery current changes very little for changes in forward currents [3].

## VII. Conclusions

This paper presents a set of models for a SiC VJFET inverter from device-level to system-level. The simulations of the SiC and Si inverters indicated that the SiC inverter has a much lower junction temperature, much less power loss, significantly enhanced energy efficiency, and a dramatic reduction in heatsink size as compared with the Si converter. This sufficiently demonstrated the technical feasibility and benefits of a SiC inverter. In the future, system experiments will be conducted in order to further validate the models presented.

## References


[1] M. Roschke, “Electron mobility models for 4H, 6H, and 3C SiC,” *IEEE Transactions on Electron Devices*, vol. 48, no.7, July 2001, pp. 1442-1447.

[2] S. Selberherr, Analysis and Simulation of Semiconductor Devices, Springer-Verlag/Wien, New York, 1984.

[3] L. M. Tolbert, B. Ozpineci, S. Islam, M. Hasanuzzaman, "Effects of silicon carbide (SiC) power devices on HEV PWM Inverter Losses," *IEEE Industrial Electronics Conference*, Nov 29 - Dec 2, 2001, Denver, Colorado, pp. 1061-1066.

[4] A. Q. Huang, B. Zhang, “Comparing SiC switching power devices: MOSFET, NPN transistor and GTO thyristor,” *Solid-State Electronics*, vol. 44, 2000, pp. 325-340.

[5] V. Blasko, R. Lukaszewski, R. Sladky, “On line thermal model and thermal management strategy of a three phase voltage source inverter,” *IEEE Industry Application Societ Annual Meeting*, October 3-7, 1999, Phoenix, Arizona, pp.1423-1431.

[6] N. Mohan, T. M. Undeland, W. P. Robbins, *Power Electronics*, 2nd ed., John Wiley & Sons Inc., 1995.

[7] M. Chinthavali, B. Ozpineci, L. M. Tolbert, “High Temperature and High Frequency Performance Evaluation of 4H-SiC Unipolar Devices,” *IEEE Applied Power Electronics Conference*, March 6-10, 2005, Austin, Texas, pp. 322-328.


## Appendix — Symbols

| Symbol | Description | Symbol | Description |
|---|---|---|---|
| $V_B$ | Breakdown voltage | $V_{GH}$ | Highest gate voltage |
| $E_c$ | Breakdown electric field | $V_{GL}$ | Lowest gate voltage |
| $\mu_n$ | Electron mobility | $V_{th}$ | Threshold voltage |
| $\varepsilon$ | Relative dielectric constant | $V$ | Applied voltage |
| $N$ | Doping density | $g_m$ | Transconductance |
| $E$ | Applied electric field | $t_{rr}$ | Reverse recovery time |
| $v_s$ | Electron saturated velocity | $S$ | Snappiness factor |
| $R_D$ | On resistance of diodes | $I_R$ | Peak reverse recovery current of diodes |
| $R_{DS,on}$ | On resistance of VJFETs | | |
| $M$ | Modulation index | $V_R$ | Reverse voltage applied to the diodes |
| $\phi$ | Phase angle of the current | | |
| $f_c$ | Switching frequency | $V_D$ | Constant part of diodes forward voltage |
| $T$ | Temperature | | |
| $T_0$ | Room temperature, 300$K$ | $R$ | Thermal resistance |
| $I$ | Current | $C$ | Thermal capacitance |
| $J$ | Current density | $\tau$ | Thermal constant |